Pergamon

0005-1098(94)00090-5

Automatica, Vol. 31, No. 2, pp. 183–199, 1995

0005-1098/95 $9.50 + 0.00

Design of Ride Control System for Surface Effect Ships using Dissipative Control*

A. J. SØRENSEN† and O. EGELAND‡

Dissipative control is used to design a ride control system for surface effect ships for active damping of vertical accelerations caused by resonances in the air cushion. Full-scale experiments showed significant improvement in ride quality.

Key Words—Marine systems; SES; vibration control; ride control; passivity; modelling.

Abstract—A ride control system for active damping of heave and pitch accelerations of surface effect ships (SES) is presented. It is demonstrated that distributed effects that are a result of spatially varying pressure in the air cushion result in significant vertical vibrations in low and moderate sea states. In order to achieve high quality human comfort and crew workability it is necessary to damp these vibrations using a control system which accounts for distributed effects owing to spatial pressure variations in the air cushion. To develop such a ride control system a mathematical model describing the motion of the craft in the vertical plane is derived. This mathematical model accounts for accelerations induced by both the dynamic uniform and the spatially varying air cushion pressure. Sensor and actuator placement is discussed, and the stability of the control system is analysed using the theory of passivity. The performance of the ride control system is shown by power spectra of the vertical accelerations and the pressure variations obtained from full-scale experiments with a 35 m SES.

1. INTRODUCTION

Surface effect ships (SES) are known to offer a high quality ride in heavy sea states compared to conventional catamarans. However, in low and moderate sea states there are problems with discomfort owing to high frequency vertical accelerations induced by resonances in the pressurized air cushion. A high performance ride control system is required in order to achieve satisfactory passenger comfort and crew workability. To develop such a ride control system it is essential to use a sufficiently detailed dynamic model. Previous ride control systems have been based on the coupled equations of motion in heave and pitch as derived by Kaplan and Davis (1974, 1978), and Kaplan *et al.* (1981). Their work was based on the assumption that the major part of the wave-induced loads from the sea was imparted to the craft as dynamic uniform air pressure acting on the wetdeck, while a minor part of the wave-induced loads from the sea was imparted to the craft as dynamic water pressure acting on the side-hulls. This work was extended by Sørensen *et al.* (1992, 1993), who included the effect of spatial pressure variations in the air cushion. It was found that acoustic resonances in the air cushion excited by incident sea waves can result in significant vertical vibrations. To investigate the acoustic resonances a distributed model was derived from a boundary value problem formulation where the air flow was represented by a velocity potential subject to appropriate boundary conditions on the surfaces enclosing the air cushion volume. A solution was found using the Helmholtz equation in the air cushion region. In Sørensen *et al.* (1992) the first two acoustic modes were included in the mathematical model, while in Sørensen *et al.* (1993) a more general model with an infinite number of acoustic modes was derived. In this paper the mathematical model presented in Sørensen *et al.* (1993) is slightly modified and adapted to control system design. This mathematical model is used to derive a new ride control system, which provides active damping of both the dynamic uniform pressure and the acoustic resonances in the air cushion. Special attention is given to sensor and actuator placement to achieve robust stability and high performance. The stability of the control system is analysed using the theory of passive systems as presented in Desoer and Vidyasagar (1975) and in Vidyasagar (1993). It is demonstrated that under appropriate assumptions the dynamic

* Received 5 July 1993; received in final form 2 June 1994. This paper was not presented at any IFAC meeting. This paper was recommended for publication in revised form by Associate Editor J. C. Kantor under the direction of Editor Y. Arkun. Corresponding author Dr Asgeir J. Sørensen. Tel. +47 22 35 94 66; Fax +47 22 35 36 80; E-mail asgeirsorensen@noina.abb.telemax.no.

† ABB Corporate Research Norway, P.O. Box 90, N-1361 Billingstad, Norway.

‡ Department of Engineering Cybernetics, The Norwegian Institute of Technology, N-7034 Trondheim, Norway.

system to be controlled is passive, and L_2^n stability can be achieved using a strictly passive controller with finite gain.

The paper is organized as follows: in Section 2 the mathematical model is derived. Section 3 includes the controller design and the stability analysis. Finally, in Section 4, simulation results and power spectra of pressure variations and vertical acceleration obtained from full-scale trials with a 35 m SES are presented.

2. MATHEMATICAL MODELLING

A moving coordinate frame is defined so that the origin is located in the mean water plane below the centre of gravity with the x-, y- and z-axes oriented positive forwards, to the port, and upwards, respectively (Fig. 1). This type of coordinate frame is commonly used in marine hydrodynamics to analyse vertical motions and accelerations (Faltinsen, 1990). The equations of motion are formulated in this moving frame. Translation along the z-axis is called heave and is denoted by $\eta_3(t)$. The rotation angle around the y-axis is called pitch and is denoted by $\eta_5(t)$. Heave is defined positive upwards, and pitch is defined positive with the bow down. We are mainly concerned about the high frequency vertical vibrations. In this frequency range the hydrodynamic loads on the slender side-hulls are of minor importance. Strip theory is used and hydrodynamic memory effects are assumed to be negligible due to the high frequency of oscillation. Furthermore, infinite water depth is assumed.

The craft is assumed to be advancing forward in regular head sea waves. The waves are assumed to have a small wave slope with circular frequency ω_o. The circular frequency of encounter ω_e is

$$\omega_e = \omega_o + kU, \tag{1}$$

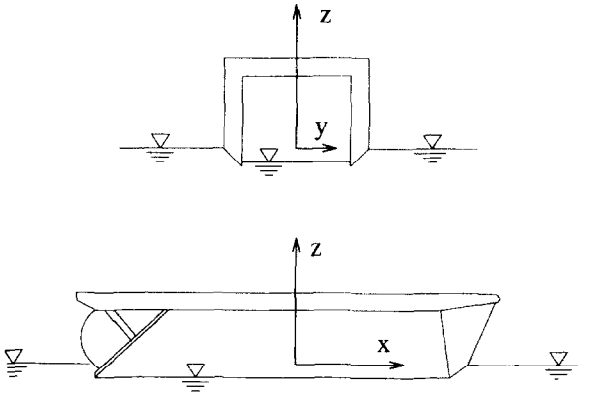

Fig. 1. Surface effect ship (SES)—coordinate frame.

where $k = 2\pi/\lambda$ is the wave number, λ is the sea wave length and U is the craft speed. The circular frequency of encounter ω_e is the apparent wave frequency as experienced on the craft advancing forward at the speed U in head sea. The incident surface wave elevation $\zeta(x, t)$ for regular head sea is defined as

$$\zeta(x, t) = \zeta_a \sin(\omega_e t + kx), \tag{2}$$

where ζ_a is the wave elevation amplitude. In the case of calm water the wave elevation amplitude is equal to 0. The water waves are assumed to pass through the air cushion undisturbed. For simplicity a rectangular cushion is considered at the equilibrium condition with height h_o, beam b and length L, reaching from $x = -L/2$ at the stern (AP) to $x = L/2$ at the bow (FP). The beam and the height of the air cushion are assumed to be much less than the length. Hence, a one-dimensional ideal and compressible air flow in the x-direction is assumed. This means that the longitudinal position of the centre of air cushion pressure is assumed to coincide with the origin of the coordinate frame. The air cushion area is then given by $A_c = Lb$. The total pressure $p_c(x, t)$ in the air cushion is represented by

$$p_c(x, t) = p_a + p_u(t) + p_{sp}(x, t), \tag{3}$$

where p_a is the atmosphere pressure, $p_u(t)$ is the uniform excess pressure and $p_{sp}(x, t)$ is the spatially varying excess pressure. The basic thermodynamic variations in the air cushion are assumed to be adiabatic. When neglecting seal dynamics, aerodynamics and viscous effects, the external forces are given by the water pressure acting on the side-hulls and by the dynamic air cushion pressure acting on the wetdeck. It is assumed that the dynamic cushion pressure is excited by incoming sea wave disturbances. In the absence of waves, the stationary excess pressure in the air cushion is equal to the equilibrium excess pressure p_o. The nondimensional uniform pressure variations $\mu_u(t)$ and the nondimensional spatial pressure variations $\mu_{sp}(x, t)$ are defined according to

$$\mu_u(t) = \frac{p_u(t) - p_o}{p_o}, \quad \mu_{sp}(x, t) = \frac{p_{sp}(x, t)}{p_o}. \tag{4}$$

The volumetric air flow into the air cushion is given by a linearization of the fan characteristic curve about the craft equilibrium operating point. It is assumed that there are q fans with constant rpm feeding the cushion, where fan i is located at the longitudinal position x_{Fi}. The volumetric air flow out of the air cushion is proportional to the leakage area $A_L(t)$, which is

defined as

$$A_L(t) = A_o + A^{RCS}(t). \quad (5)$$

$A_L(t)$ represents the total leakage area and is expressed as the sum of an equilibrium leakage area A_o and a controlled variable leakage area $A^{RCS}(t)$. The equilibrium leakage area

$$A_o = A_o^{AP} + A_o^{FP} \quad (6)$$

will be divided into leakage areas under the bow and stern region or more precisely under the stern and bow seals. A_o^{AP} is the stern equilibrium leakage area at $x = -L/2$ and A_o^{FP} is the bow equilibrium leakage area at $x = L/2$. The controlled leakage area $A^{RCS}(t)$ of the ride control system is written

$$A^{RCS}(t) = \sum_{i=1}^{r} (A_{oi}^{RCS} + \Delta A_i^{RCS}(x_{si}, t)), \quad (7)$$

where r is the number of louvers. The louvers are variable vent valves located at the longitudinal position $x = x_{Li}$, which change the area of openings in the wetdeck for the purpose of leakage control. A_{oi}^{RCS} is defined as the mean operating value or bias of the leakage area and $\Delta A_i^{RCS}(x_{si}, t)$ is defined as the commanded variable leakage area of louver i. Pressure sensors are used to measure the pressure variations in the air cushion. Sensor i is placed at the longitudinal position $x = x_{si}$. Dynamic leakage areas under the side-hulls and the seals owing to craft motion are assumed to be negligible in this analysis. This type of leakage is a hard nonlinearity and can be analysed using describing functions (Gelb and Vander Velde, 1968). Computer simulations done in Sørensen *et al.* (1992) indicate that the dynamic leakage terms owing to craft motion can be neglected for small amplitudes of sea wave disturbances and associated small amplitudes of heave and pitch motions, as long as the sealing ability is good.

2.1. *Boundary value problem for spatial pressure variations*

The effect of spatial pressure variations in the air cushion was investigated by Sørensen *et al.* (1992, 1993) in the frequency domain using Helmholtz equation. In this paper the wave equation is considered leading to a more general solution formulated in the time domain. A distributed model is derived from a boundary value problem formulation. A one-dimensional ideal and compressible air flow in the x-direction is assumed. The motion of the craft in the vertical plane is assumed to be small so the body boundary conditions and the free surface condition can be linearized. The air flow dynamics is formulated in terms of potential theory. The velocity potential $\phi_{sp}(x, z, t)$ for the spatially varying pressure is assumed to satisfy the wave equation in the cushion region and the boundary conditions enclosing the cushion volume (Fig. 2). The wave equation is given by

$$\frac{\partial^2 \phi_{sp}(x, z, t)}{\partial t^2} - c^2\left(\frac{\partial^2 \phi_{sp}(x, z, t)}{\partial x^2} + \frac{\partial^2 \phi_{sp}(x, z, t)}{\partial z^2}\right) = 0, \quad (8)$$

where c is the speed of sound in air. The one-dimensional approximation of the velocity potential is introduced

$$\psi_{sp}(x, t) = \frac{1}{h_o}\int_0^{h_o} \phi_{sp}(x, z, t)\, dz. \quad (9)$$

By integrating the wave equation in the z-direction, the following partial differential equation of second-order in the two variables x and t is obtained

$$\frac{c^2}{h_o b}\int_{-b/2}^{b/2} dy\left(\frac{\partial \phi_{sp}(x, z, t)}{\partial z}\bigg|_{z=h_o} - \frac{\partial \phi_{sp}(x, z, t)}{\partial z}\bigg|_{z=0}\right) + c^2\frac{\partial^2 \psi_{sp}(x, t)}{\partial x^2} - \frac{\partial^2 \psi_{sp}(x, t)}{\partial t^2} = 0. \quad (10)$$

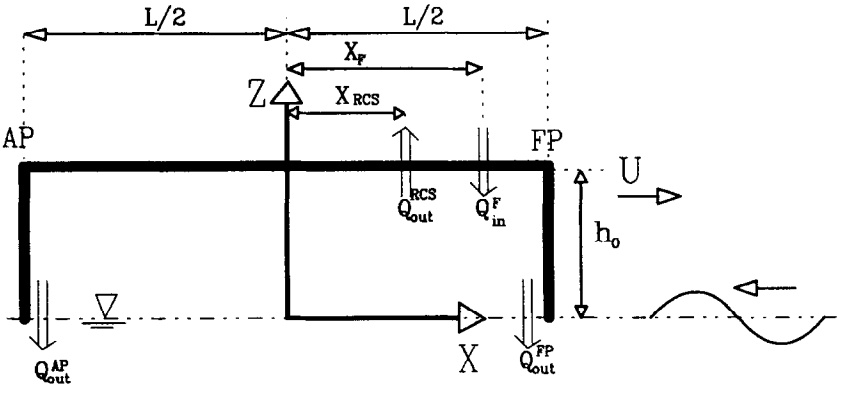

Fig. 2. The boundary value problem.

It is then possible to derive an analytical solution of the boundary value problem. Because the louver area and the outflow area of the lift fan system do not cover the whole beam, it is necessary to integrate these boundary conditions in the y-direction. The nondimensional spatial pressure variations $\mu_{sp}(x, t)$ can be found as

$$\mu_{sp}(x, t) = -\frac{\rho_{co}}{p_o}\frac{\partial \psi_{sp}(x, t)}{\partial t}. \tag{11}$$

The unbounded differential operator $\partial^2/\partial x^2$ with boundary conditions on the finite interval $x \in [-L/2, L/2]$ appearing in (10) has a set of discrete eigenvalues (Keener, 1988) called the discrete spectrum of the differential operator. $\partial^2/\partial x^2$ is a time-invariant smooth, self-adjoint differential operator which is dense in the infinite-dimensional inner product space $L_2(\Omega)$, where Ω denotes the air cushion. $L_2(\Omega)$ is complete and hence a Hilbert space. The eigenvalue equation is given by

$$-c^2\frac{\partial^2}{\partial x^2}(r_j(x)) = \omega_j^2 r_j(x), \quad j = 1, 2, 3, \ldots, k, \tag{12}$$

where $r_j(x)$ is the eigenfunction or the mode shape function of mode j, and ω_j is the corresponding eigenfrequency. The eigenfunctions for $j \in \{1, 2, 3, \ldots, k\}$ are orthonormal, that is

$$(r_i(x), r_j(x)) = \int_{-L/2}^{L/2} r_i(x) r_j(x)\, dx = \delta_{ij}, \tag{13}$$

where $(\cdot, \cdot)$ denotes the scalar product. The Kronecker delta is defined by $\delta_{ij} = 1$ when $i = j$ and $\delta_{ij} = 0$ when $i \neq j$. Letting $k \to \infty$, the eigenfunctions $r_j(x)$ for $j \in \{1, 2, 3, \ldots\}$ form an orthonormal basis of the Hilbert space $L_2(\Omega)$. Thus, $\mu_{sp}(x, t)$ has a unique modal representation for $k \to \infty$ given by

$$\mu_{sp}(x, t) = -\frac{\rho_{co}}{p_o}\sum_{j=1}^{\infty}\frac{\partial \psi_j^i(t)}{\partial t}\psi_j^x(x) = \sum_{j=1}^{\infty}\dot{p}_j(t) r_j(x), \tag{14}$$

where the time derivatives of $p_j(t)$ is the modal amplitude function for mode j and $\psi_j^x(x) = r_j(x)$. Owing to linearity and orthogonality between the modes, each mode can be considered separately and the contributions from each of them are superposed. In Appendix B the boundary conditions on the surfaces enclosing the cushion air volume are defined. The mode shape functions will be chosen so the boundary conditions on the seals are satisfied. The following mode shape functions, in general infinitely many, will satisfy the boundary condition on the seals

$$r_j(x) = \cos\frac{j\pi}{L}\left(x + \frac{L}{2}\right), \quad x \in \left[-\frac{L}{2}, \frac{L}{2}\right], \quad j = 1, 2, 3, \ldots. \tag{15}$$

From (12) we find that the corresponding eigenfrequency ω_j for mode j is

$$\omega_j = c\frac{j\pi}{L}, \quad j = 1, 2, 2, \ldots. \tag{16}$$

The modal amplitude functions will be determined according to (10) and the remaining boundary conditions. By taking the inner product of (10) with the mode shape function of mode j for $j \in \{1, 2, 3, \ldots\}$ and using (14), we find the spatially varying pressure equation for mode j for $j \in \{1, 2, 3, \ldots\}$ (see (22) and (25) later in the text). The heave force and the pitch moment owing to the spatially varying pressure are found in the following way:

$$F_3^{sp}(t) = p_o b \int_{-L/2}^{L/2}\sum_{j=1}^{\infty}\dot{p}_j(t) r_j(x)\, dx = 0, \quad j = 1, 2, 3, \ldots,$$

$$F_5^{sp}(t) = -p_o b \int_{-L/2}^{L/2}\sum_{j=1}^{\infty}\dot{p}_j(t) r_j(x) x\, dx = \begin{cases} 2p_o b \sum_{j=1,3,\ldots}\left(\frac{L}{j\pi}\right)^2\dot{p}_j, & j = 1, 3, 5, \ldots \\ 0, & j = 2, 4, 6, \ldots. \end{cases} \tag{17}$$

Owing to symmetry around the origin, there is no contribution from the spatially varying pressure on the heave motion. However, the pitch moment $F_5^{sp}(t)$ is important to include in the pitch equation.

2.2. *Equations of motion and dynamic cushion pressure*

The coupling between the dynamic uniform pressure and the spatially varying pressure and hydrodynamic and hydrostatic coupling terms like A_{ij}-, B_{ij}- and C_{ij}-terms are assumed to be negligible regarding control system design. The equations of motions and the dynamic air cushion pressure are:

(1) Uniform pressure equation

$$K_1\dot{\mu}_u(t) + K_3\mu_u(t) + \rho_{co}A_c\dot{\eta}_3(t) = K_2\sum_{i=1}^{r}\Delta A_i^{RCS}(x_{si}, t) + \rho_{co}\dot{V}_0(t), \tag{18}$$

where the time derivative of $V_o(t)$ is the wave

volume pumping and is found in the following way for regular head sea waves:

$$\dot{V}_0(t) = b\int_{-L/2}^{L/2} \dot{\zeta}(x,t)\,dx = A_c\zeta_a\omega_e \frac{\sin\frac{kL}{2}}{\frac{kL}{2}}\cos\omega_e t \tag{19}$$

and

$$K_1 = \frac{\rho_{co}h_o A_c}{\gamma\left(1+\frac{p_a}{p_o}\right)},\quad K_2 = \rho_{co}c_n\sqrt{\frac{2p_o}{\rho_a}},\quad K_3 = \rho_{co}\sum_{i=1}^{q}\left(\frac{Q_{oi}}{2} - p_o\left.\frac{\partial Q}{\partial p}\right|_{oi}\right), \tag{20}$$

where ρ_a is the air density at the atmospheric pressure p_a, ρ_{co} is the density of the air at the equilibrium pressure p_o, γ is the ratio of specific heat for air, Q_{oi} is the equilibrium air flow rate of fan i when $p_u(t) = p_o$ and $(\partial Q/\partial p)|_{oi}$ is the corresponding linear fan slope about the craft equilibrium operating point Q_{oi} and p_o of fan i. c_n is the orifice coefficient varying between 0.61 and 1 depending on the local shape on the edges of the leakage area. In the numerical simulations $c_n = 0.61$ is used.

(2) Spatially varying pressure equation

$$\mu_{sp}(x,t) = \sum_{j=1}^{\infty}\dot{p}_j(t)\cos\frac{j\pi}{L}\left(x+\frac{L}{2}\right),\quad x\in\left[-\frac{L}{2},\frac{L}{2}\right]. \tag{21}$$

Odd modes around the centre of pressure, $j = 1, 3, 5, \ldots$

$$\ddot{p}_j(t) + 2\xi_j\omega_j\dot{p}_j(t) + \omega_j^2 p_j(t) = -c_{2j}\dot{\eta}_5(t) + c_1\sum_{i=1}^{r}\cos\frac{j\pi}{L}\times\left(x_{Li}+\frac{L}{2}\right)\Delta A_i^{RCS}(x_{si},t) + \rho_{co}\dot{V}_j(t), \tag{22}$$

where

$$c_1 = \frac{2K_2c^2}{p_oV_{co}},\quad c_{2j} = \frac{4\rho_{co}Lc^2}{p_oh_o(j\pi)^2}. \tag{23}$$

The wave volume pumping for regular head sea for $j = 1, 3, 5, \ldots$, is

$$\dot{V}_j(t) = -\frac{4c^2}{p_oh_oL}\frac{k\cos\frac{kL}{2}}{k^2-\left(\frac{j\pi}{L}\right)^2}\omega_e\zeta_a\sin\omega_e t. \tag{24}$$

Even modes around the centre of pressure, $j = 2, 4, 6, \ldots$

$$\ddot{p}_j(t) + 2\xi_j\omega_j\dot{p}_j(t) + \omega_j^2 p_j(t) = c_1\sum_{i=1}^{r}\cos\frac{j\pi}{L}\times\left(x_{Li}+\frac{L}{2}\right)\Delta A_i^{RCS}(x_{si},t) + \rho_{co}\dot{V}_j(t), \tag{25}$$

where the wave volume pumping for regular head sea for $j = 2, 4, 6, \ldots$, is

$$\dot{V}_j(t) = \frac{4c^2}{p_oh_oL}\frac{k\sin\frac{kL}{2}}{k^2-\left(\frac{j\pi}{L}\right)^2}\omega_e\zeta_a\cos\omega_e t. \tag{26}$$

The relative damping ratio for $j = 1, 2, 3, 4, \ldots$, is

$$\xi_j = \frac{c}{j\pi h_o b}\left(\frac{K_2}{2p_o}A_o + \frac{K_2}{2p_o}\sum_{i=1}^{r}A_{oi}^{RCS}\cos^2\frac{j\pi}{L}\times\left(x_{Li}+\frac{L}{2}\right) - \rho_{co}\sum_{i=1}^{q}\left.\frac{\partial Q}{\partial p}\right|_{oi}\cos^2\frac{j\pi}{L}\times\left(x_{Fi}+\frac{L}{2}\right)\right). \tag{27}$$

(3) Heave equation

$$(m+A_{33})\ddot{\eta}_3(t) + B_{33}\dot{\eta}_3(t) + C_{33}\eta_3(t) - A_cp_o\mu_u(t) = F_3^e(t), \tag{28}$$

where m is the craft mass.

(4) Pitch equation

$$(I_{55}+A_{55})\ddot{\eta}_5(t) + B_{55}\dot{\eta}_5(t) + C_{55}\eta_5(t) - 2p_ob\sum_{j=1,3,\ldots}\left(\frac{L}{j\pi}\right)^2\dot{p}_j(t) = F_5^e(t), \tag{29}$$

where I_{55} is the moment of inertia around the y-axis.

The hydrostatic C_{ii} terms are found in the standard way by integration over the water plane area of the side-hulls. The hydrodynamic added-mass coefficients A_{ii}, the water wave radiation damping coefficients B_{ii}, and the hydrodynamic excitation force in heave $F_3^e(t)$ and moment in pitch $F_5^e(t)$, are derived from hydrodynamic loads on the side-hulls. The hydrodynamic loads on the side-hulls may be calculated as presented in Nestegård (1990), Faltinsen and Zhao (1991a, b) and Faltinsen *et al.* (1991, 1992). However, since the main focus in this paper is on the high frequency range, we have used a simplified strip theory based on Salvesen *et al.* (1970) for calculation of the hydrodynamic loads. Neglecting the effects of transom stern and radiation damping, the hydrodynamic excitation forces on the side-hulls

in heave and pitch are given by

$$F_3^e(t) = 2\zeta_a e^{-kd} \frac{\sin\frac{kL}{2}}{\frac{kL}{2}} (C_{33} - \omega_o \omega_e A_{33}) \sin \omega_e t, \tag{30}$$

$$F_5^e(t) = 2\zeta_a e^{-kd} \left[\left(\frac{1}{k} \cos\frac{kL}{2} - \frac{2}{k^2 L} \sin\frac{kL}{2} \right) \times (C_{33} - \omega_o \omega_e A_{33}) - U\omega_o \times \frac{\sin\frac{kL}{2}}{\frac{kL}{2}} A_{33} \right] \cos \omega_e t, \tag{31}$$

where d is the draft of the side-hulls. In the case studied here, the submerged part of the side-hulls are assumed to have constant cross-sectional area. Examples of two-dimensional frequency depending added-mass and wave radiation damping coefficients are found in Faltinsen (1990). In the control system analysis constant two-dimensional B_{ii} and A_{ii} values are assumed. The high frequency limit of the two-dimensional added-mass coefficient found in Faltinsen (1990) is used. The selected wave radiation damping coefficient in pitch corresponds to the value at the pitch resonance frequency determined from structural mass forces acting on the craft and hydrodynamic forces on the side-hulls. For heave we have chosen the wave radiation damping coefficient at the resonance frequency that will exist without the presence of the excess air cushion pressure. These simplifications are motivated by fact that the effect of damping is most pronounced around the corresponding resonance frequency.

2.3. *Discussion of the mathematical model*

It is seen from (28) and (29) that the heave and pitch motions are coupled to the dynamic excess pressure in the air cushion region. This is to be expected since the major part of the SES mass is supported by the air cushion excess pressure. The dynamic air cushion pressure is expressed as the sum of the dynamic uniform pressure and the spatially varying pressure. An important question is how many acoustic modes should be included in the mathematical model. Even if the solution is formally presented by an infinite number of acoustic modes, the modelling assumptions will not be valid in the high frequency range when two- and three-dimensional effects become significant. Then a more detailed numerical analysis is required, like for instance a boundary element or a finite element method. In the following we will use a finite number k of acoustic modes in the mathematical model. The effect of higher order modes is assumed to be negligible. It is important to note that the air cushion dimensions and the forward speed affect the energy level of the vertical accelerations caused by the acoustic resonances. The acoustic resonance frequencies are inversely proportional to the air cushion length as seen from (16). The wave excitation frequency which is given by the circular frequency of encounter, $\omega_e = \omega_o + kU$, increase with the forward speed U. Thus waves of relatively low circular frequency ω_o may excite the craft in the frequency range of the acoustic resonance when the speed U is high. This may result in more energy in the sea wave excitation around the resonance frequencies since the maximum sea wave height will tend to increase when the period of the sea waves increases. The relative damping ratio ξ_j given by (27) is an important parameter. As expected the leakage terms and the fan inflow term contribute to increased damping. One should notice that the fan slope $(\partial Q/\partial p)|_{\omega_j}$ is negative. We also observe that the longitudinal placement of the fan and the louver systems strongly affects the relative damping ratio. In the case of a single fan system and a single louver system, it may seem natural to place the fan and the louver in the middle of the air cushion, that is $x_F = x_L = 0$. However, from (27) we observe that the relative damping ratio for the odd modes will be reduced significantly if x_L and x_F are equal to 0. Maximum damping of both the odd and even acoustic resonance modes in the case of a single lift fan system and a single louver system is obtained for x_F and x_L equal to $-L/2$ or $L/2$. The relative damping ratio of the first odd acoustic mode on a 35 m SES will increase from about 0.05 to 0.2 by placing the lift fan system at one of the ends of the air cushion instead of in the middle. This gives a significant improvement in ride quality even when the ride control system is turned off. In the same manner the active damping due to the ride control system is maximized by placing the louver system at one of the ends of the air cushion.

3. ROBUST DISSIPATIVE CONTROLLER DESIGN

In this section a ride control system based on the mathematical model derived in the previous section is developed. The objective of the controller is to damp out pressure fluctuations around the equilibrium pressure p_o in the

presence of sea wave disturbances. This can be formulated in terms of the desired value of the nondimensional dynamic uniform pressure $\mu_u^d(t) = 0$ and the nondimensional spatially varying pressure $\mu_{sp}^d(x, t) = 0$, where the superscript d denotes the desired value. The number of modes to be damped depends on the requirements related to established criteria for crew workability and passenger comfort. The mathematical model of the craft dynamics is of high order as it contains a high number of acoustic modes. A practical implementable controller has to be of reduced order. When designing a controller based on a reduced-order model, it may happen that the truncated or residual modes result in degradation of the performance, and even instability of the closed-loop system. This is analogous with the so-called spillover effect in active damping of vibrations in mechanical structures (Balas, 1978). The inadvertent excitation of the residual modes has been termed control spillover, while the unwanted contribution of the residual modes to the sensed outputs has been termed observation spillover (Fig. 3). This problem was also discussed by Gevarter (1970) in connection with control of flexible vehicles. Mode 0 in Fig. 3 is related to the uniform pressure, while the higher-order modes are related to the spatially varying pressure. The controller must be robust with respect to modelling errors and parametric and nonparametric uncertainties, nonlinearities in sensors and actuators, and component failure.

The use of collocated compatible actuators and sensors pairs, and strictly passive controllers provides a design technique for circumventing these problems. The louver and sensor pairs are distributed along the air cushion, preferentially in the longitudinal direction. The problem described in this paper is closely related to the problem of vibration damping in large flexible space structures. Inspired by the work of Joshi (1989) we propose to use dissipative control for vibration damping of SES. Note that the problem of vibration damping of SES has significant differences as the dynamic system given by (18)–(31) is of third-order as opposed to similar vibration damping problems of large flexible space structures that can be written as an equivalent second-order mass, damper and spring system. Also, we use passivity theory in the following, whereas Joshi (1989) used Lyapunov theory. In dissipative controller synthesis using a linear design model it is possible to use standard linear synthesis methods, however, the design is complicated by the constraint that the resulting controller must satisfy appropriate passivity properties. In the present paper a static dissipative solution is presented where a passive controller with proportional feedback is used. It would also be possible to use dynamic dissipative control based on LQG synthesis (Lozano-Leal and Joshi, 1988; Joshi and Maghami, 1990; Joshi *et al.* 1991) or H^∞ control synthesis (Haddad *et al.*, 1993). It is straightforward to extend the stability results

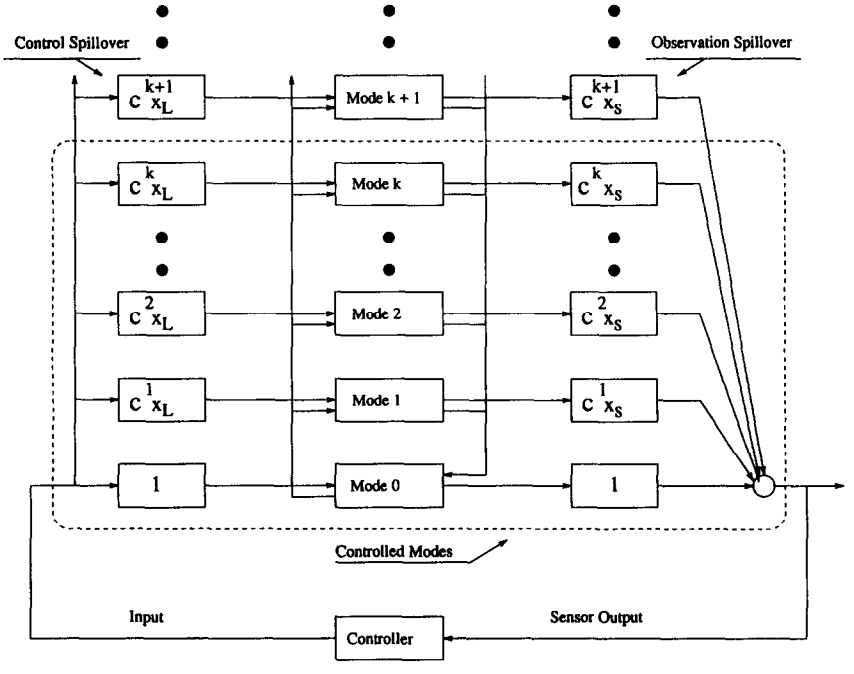

Fig. 3. Observation and control spillover, where $C^k x_L = \cos k\pi(x_L + L/2)/L$ and $C^k x_s = \cos k\pi(x_s + L/2)/L$.

presented in the following to the case of dynamic dissipative controllers.

3.1. *Preliminaries*

The linear vector space L_2^n of real square-integrable n vector functions of time t is defined by

$$L_2^n = \left\{ z : R_+ \to R^n \;\middle|\; \int_0^\infty z(t)^T z(t)\, dt < \infty \right\}. \quad (32)$$

Define the truncation operator P_T such that

$$z_T = P_T z = \begin{cases} z(t) & 0 \le t \le T \\ 0 & t > T \end{cases}. \quad (33)$$

The extended space L_{2e}^n is then defined as

$$L_{2e}^n = \{ z : R_+ \to R^n \mid \forall T \ge 0,\ \|z\|_{T2} < \infty \}. \quad (34)$$

The respective norms $\|\cdot\|_2$ and $\|\cdot\|_{T2}$ are defined by

$$\|z\|_2 = \lim_{T \to \infty} \|z\|_{T2}, \quad (35)$$

where

$$\|z\|_{T2} = (z, z)_T^{1/2} = \left(\int_0^T z(t)^T z(t)\, dt \right)^{1/2}. \quad (36)$$

The inner product $(\cdot, \cdot)$ of $x, z \in L_{2e}^n$ is

$$(x, z)_T = \int_0^T x(t)^T z(t)\, dt \quad (37)$$

so that $\|z\|_{T2}^2 = (z, z)_T$. If $x, z \in L_2^n$, then

$$(x, z) = \lim_{T \to \infty} (x, z)_T \quad (38)$$

and hence $\|z\|_2^2 = (z, z)$. A function $z : R_+ \to R^n$ belongs to L_∞^n if

$$\|z\|_\infty = \operatorname*{ess\,sup}_{t \ge 0} |z(t)| < \infty. \quad (39)$$

By essential supremum we mean

$$\operatorname*{ess\,sup}_{t \ge 0} |z(t)| = \inf_{t \ge 0} \times \{ a \mid |z(t)| \le a \text{ almost everywhere} \}, \quad (40)$$

that is $|z(t)| \le a$ except for a set of measure zero, and the ess sup is the smallest number which has that property. Notice that the L_∞^n space is a normed linear space but not an inner product space. Disturbances induced by irregular sea, and regular sea as well, are persistent for a long period of time and can be represented by sinusoidals. This is the case in (19), (24), (26), (30) and (31). Such disturbances belong to the L_∞^n space but not to the L_2^n space. On the other hand, in regular sea over a finite time interval when for example running the craft into and out of a wave field set up by the craft itself or by other ships, the disturbances are transient and may belong to the L_2^n space. This may be modelled using the truncation operator given in (33) on the (19), (24), (26), (30) and (31). Passivity and strict passivity on L_{2e}^n are defined below

Definition 1. (Desoer and Vidyasagar, 1975). Let $H : L_{2e}^n \to L_{2e}^n$. H is passive if there exists some constant β such that

$$(Hu, u)_T \ge \beta, \quad \forall u \in L_{2e}^n, \quad \forall T \ge 0. \quad (41)$$

H is strictly u-passive if there exist some $\delta_2 > 0$ and some constant β such that

$$(Hu, u)_T \ge \delta_2 \|u\|_{T2}^2 + \beta, \quad \forall u \in L_{2e}^n, \quad \forall T \ge 0. \quad (42)$$

Definition 2. (Desoer and Vidyasagar, 1975). Let $H : L_{pe}^n \to L_{pe}^n$. The mapping H is L_p^n stable with finite gain if $Hu \in L_p^n$ whenever $u \in L_p^n$ and there exist finite constants γ and α such that

$$\|Hu\|_p \le \gamma \|u\|_p + \alpha, \quad \forall u \in L_p^n, \quad p \in [1, \infty]. \quad (43)$$

If $\alpha = 0$, the mapping H is L_p^n stable with finite gain and zero bias.

3.2. *State space model*

The dynamic system given by (18)–(31) is written in standard state space form

$$\begin{aligned} \dot{x}(t) &= Ax(t) + Bu(t) + Ev(t), \\ y(t) &= Cx(t), \end{aligned} \quad (44)$$

where the n-dimensional state vector $x(t)$ is

$$x(t) = [\eta_3, \eta_5, \dot{\eta}_3, \dot{\eta}_5, \mu_u, p_1, p_2, \ldots, p_k, \dot{p}_1, \dot{p}_2, \ldots, \dot{p}_k]^T, \quad (45)$$

$v(t)$ is the $(3 + k)$-dimensional disturbance vector defined as

$$v(t) = [F_3^e, F_5^e, \dot{V}_0, \dot{V}_1, \dot{V}_2, \ldots, \dot{V}_k]^T \quad (46)$$

where $F_3^e(t)$, $F_5^e(t)$ and the time derivative of $V_i(t)$ for $i = 0, 1, 2, \ldots, k$ are found in Section 2. k is the number of acoustic modes, $u(t)$ is the r-dimensional control input vector, and r is the number of louvers. The elements of $u(t)$ are, for $i = 1, 2, \ldots, r$

$$u_i(t) = \Delta A_i^{RCS}(x_{si}, t), \quad (47)$$

where $\Delta A_i^{RCS}(x_{si}, t)$ is defined in (7). $y(t)$ is the m-dimensional measurement vector and m is the number of pressure sensors. The symbolic expressions for the $n \times n$ system matrix A, $n \times r$ control input matrix B, $n \times (3 + k)$ disturbance matrix E and $m \times n$ measurement matrix C are given in Appendix C. Consider the case where

sensors and actuators are ideal, that is linear and instantaneous with no noise. It is assumed that the control input matrix B can be related to the measurement matrix C so that

$$C = B^{\mathrm{T}}P, \tag{48}$$

where P is a $n \times n$ symmetric positive definite matrix providing correct scaling of the B^{T} matrix to the C matrix. This is the case when there is perfect collocation between the sensors and the louvers, i.e. $x_{Li} = x_{si}$ for all i and $r = m$. We can derive the linear time-invariant operators between the outputs and the inputs of the dynamic system given by (44). Denote s to be the different operator. Since the pair (A, B) is controllable and the pair (A, C) is observable, the dynamic system can be represented by

$$\begin{aligned} \boldsymbol{y}(s) &= H_p(s)\boldsymbol{u}(s) + H_d(s)\boldsymbol{v}(s) \\ &= \boldsymbol{y}_u(s) + \boldsymbol{y}_v(s), \end{aligned} \tag{49}$$

where

$$\begin{aligned} H_p(s) &= C(sI_n - A)^{-1}B, \\ H_d(s) &= C(sI_n - A)^{-1}E \end{aligned} \tag{50}$$

and I_n is the $n \times n$ identity matrix.

3.3. *Stability properties of the control system*

In this section a strictly passive controller with finite gain is proposed. Employing the definitions of passivity as presented in Desoer and Vidyasagar (1975) and in Vidyasagar (1993) on an interconnected system consisting of two subsystems in a standard feedback configuration (Fig. 4), robust stability of the feedback system can be shown for certain input–output properties of the subsystems. The following lemma showing that the $n \times n$ system matrix A is Hurwitz will then be utilized.

Lemma 1. The eigenvalues of the $n \times n$ system matrix A given in (44) have negative real parts.

Proof. Consider the autonomous system of (44) with $\boldsymbol{u}(t) = \boldsymbol{v}(t) = 0$. Define the Lyapunov function candidate

$$V(\boldsymbol{x}) = \tfrac{1}{2}\boldsymbol{x}^{\mathrm{T}}P\boldsymbol{x} > 0, \tag{51}$$

where the $n \times n$ diagonal positive definite matrix

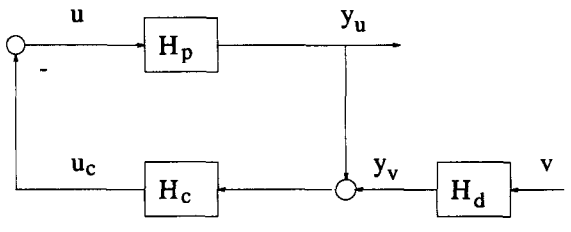

Fig. 4. Feedback system.

P is given in (56). $V(\boldsymbol{x})$ is positive definite. The time derivative of $V(\boldsymbol{x})$ along system trajectories is

$$\begin{aligned} \dot{V}(\boldsymbol{x}) &= \tfrac{1}{2}\boldsymbol{x}^{\mathrm{T}}(A^{\mathrm{T}}P + PA)\boldsymbol{x} \\ &= -\tfrac{1}{2}\boldsymbol{x}^{\mathrm{T}}Q\boldsymbol{x} \le 0. \end{aligned} \tag{52}$$

The $n \times n$ diagonal positive semidefinite matrix Q is

$$Q = \mathrm{diag}\,[0_{2\times 2}, Q1_{3\times 3}, 0_{k\times k}, Q2_{k\times k}]. \tag{53}$$

The 3×3 diagonal positive definite $Q1_{3\times 3}$ matrix is

$$\begin{aligned} Q1_{3\times 3} &= \mathrm{diag}\,[q_{ii}], \quad i = 3, 4, 5, \\ q_{33} &= p_{33}\frac{2B_{33}}{m + A_{33}}, \quad q_{44} = p_{44}\frac{2B_{55}}{I_{55} + A_{55}}, \\ q_{55} &= p_{55}\frac{2K_3}{K_1}. \end{aligned} \tag{54}$$

The $k \times k$ diagonal positive definite $Q2_{k\times k}$ matrix is

$$\begin{aligned} Q2_{k\times k} &= \mathrm{diag}\,[q_{ii}], \\ & i = 5 + k + 1, 5 + k + 2, \ldots, 5 + 2k, \\ q_{(5+k+j)(5+k+j)} &= p_{(5+k+j)(5+k+j)}4\xi_j\omega_j, \\ & j = 1, 2, 3, \ldots, k. \end{aligned} \tag{55}$$

The $n \times n$ diagonal positive definite matrix P is found from (52) to be

$$\begin{aligned} P &= \mathrm{diag}\,[p_{ii}], \quad i = 1, 2, \ldots, 5 + 2k, \\ & j = 1, 2, \ldots, k, \\ p_{11} &= p_{33}\frac{C_{33}}{m + A_{33}}, \quad p_{22} = p_{44}\frac{C_{55}}{I_{55} + A_{55}}, \\ p_{33} &= p_{55}\frac{\rho_{\mathrm{co}}(m + A_{33})}{K_1 p_{\mathrm{o}}}, \quad p_{44} = -\frac{g_1}{d_1 c_1}, \\ p_{55} &= \frac{K_1}{\rho_{\mathrm{co}}K_2}, \quad p_{(5+j)(5+j)} = \frac{\omega_j^2}{c_1}, \\ p_{(5+k+j)(5+k+j)} &= \frac{1}{c_1}, \end{aligned} \tag{56}$$

where c_1 is defined in (23). From (44) and (52) it is seen that

$$\begin{aligned} &\dot{V}(\boldsymbol{x}) = 0 \\ &\Downarrow \\ &\boldsymbol{x} = \boldsymbol{x}_0 = [\eta_3, \eta_5, 0, 0, 0, p_1, p_2, \ldots, p_k, 0, 0, \ldots, 0]^{\mathrm{T}}. \end{aligned} \tag{57}$$

However, from (44)

$$\ddot{\eta}_3 = \ddot{\eta}_5 = \dot{\mu}_{\mathrm{u}} = \dot{p}_1 = \dot{p}_2 = \cdots = \dot{p}_k = 0, \tag{58}$$

which implies

$$\eta_3 = \eta_5 = p_1 = p_2 = \cdots = p_k = 0. \tag{59}$$

Hence, by the invariant set theorem (Vidyasagar, 1993) the equilibrium point $\boldsymbol{x}_{\mathrm{o}} = 0$ is

asymptotically stable and the result of Lemma 1 follows. □

Define the linear time-invariant operators $H_p: L_{2e}^m \to L_{2e}^r (r = m)$ and $H_d: L_2^{3+k} \to L_2^m$, such that $\boldsymbol{y}_v \in L_2^m$ whenever $\boldsymbol{v} \in L_2^{3+k}$. In the following lemma it is shown that the process operator H_p is passive. This allows for the design of robust, stable output feedback controllers for ride control of SES.

Lemma 2. The process operator H_p is passive.

Proof. Set $\boldsymbol{v}(t) = 0$ in (44) and use the Lyapunov function candidate as given in (51). $V(\boldsymbol{x})$ is positive definite. The time derivative of $V(\boldsymbol{x})$ along the system trajectories is

$$\dot{V}(\boldsymbol{x}) = \tfrac{1}{2}\boldsymbol{x}^T(A^TP + PA)\boldsymbol{x} + \boldsymbol{x}^TPB\boldsymbol{u}. \quad (60)$$

The $n \times n$ diagonal positive semidefinite matrix Q is given in (53). If we assume perfect collocation between the sensor and actuator pairs, that is $C = B^TP$, (60) becomes

$$\begin{aligned}\dot{V}(\boldsymbol{x}) &= \boldsymbol{x}^TC^T\boldsymbol{u} - \tfrac{1}{2}\boldsymbol{x}^TQ\boldsymbol{x} \\ &= \boldsymbol{y}_u^T\boldsymbol{u} - \tfrac{1}{2}\boldsymbol{x}^TQ\boldsymbol{x}. \end{aligned} \quad (61)$$

Integrating (61) from $t = 0$ to $t = T$ we obtain

$$(\boldsymbol{y}_u, \boldsymbol{u})_T = V(t = T) - V(t = 0) + \frac{1}{2}\int_0^T \boldsymbol{x}^TQ\boldsymbol{x}\, dt. \quad (62)$$

Since $Q \geq 0$ and $V(t = T) > 0$, (62) can be written

$$(\boldsymbol{y}_u, \boldsymbol{u})_T \geq -V(t = 0) \triangleq \beta \quad (63)$$

and the result of Lemma 2 follows. □

Remark 1. It is evident from (44) that if the initial conditions are equal to zero, that is $\boldsymbol{x}(t = 0) = 0$, then $\beta = -1/2\boldsymbol{x}^T(t = 0)P\boldsymbol{x}(t = 0) = 0$.

Remark 2. The transfer matrix $H_d(s)$ of the linear time-invariant operator H_d as defined by (50) is strictly proper and all the poles have negative real parts according to Lemma 1. Hence, if $\boldsymbol{v} \in L_2^{3+k}$, then $\boldsymbol{y}_v = H_d\boldsymbol{v} \in L_2^m \cap L_\infty^m$.

Let the controller be defined as the linear time-invariant operator H_c between the input $\boldsymbol{y} = \boldsymbol{y}_u + \boldsymbol{y}_v$ and the output $\boldsymbol{u}_c$. Connecting the H_c operator with the H_p and H_d operators, we obtain the feedback system illustrated in Fig. 4. The transfer matrix of H_c is denoted $H_c(s)$.

Proportional control law. A strictly $\boldsymbol{u}$-passive proportional pressure feedback controller of dimension $r \times r$ with finite gain is proposed according to

$$\begin{aligned}\boldsymbol{u}_c(s) &= H_c(s)\boldsymbol{y}(s), \\ H_c(s) &= G_p, \end{aligned} \quad (64)$$

where $G_p = \text{diag}\,[g_{pi}] > 0$ is a constant diagonal feedback gain matrix of dimension $r \times r$. This control law provides enhanced damping of the pressure variations around the resonance frequencies.

The main result of this section is given by the following theorem.

Theorem 1. Consider the following feedback system (see, Fig. 4)

$$\begin{aligned}\boldsymbol{y}_u &= H_p\boldsymbol{u}, \\ \boldsymbol{y}_v &= H_d\boldsymbol{v}, \\ \boldsymbol{y} &= \boldsymbol{y}_u + \boldsymbol{y}_v, \\ \boldsymbol{u} &= -\boldsymbol{u}_c = -H_c\boldsymbol{y}, \end{aligned} \quad (65)$$

where $H_p, H_c: L_{2e}^m \to L_{2e}^m$. Assume that $H_d: L_2^{3+k} \to L_2^m$, so that $\boldsymbol{y}_v \in L_2^m$, whenever $\boldsymbol{v} \in L_2^{3+k}$. H_c is strictly $\boldsymbol{u}$-passive with finite gain and H_p is passive. Hence, the feedback system defined in (65) is L_2^m stable and since the feedback system given by H_d, H_p and H_c is linear, L_2^m stability is equivalent to L_∞^m (BIBO) stability.

Proof. Set $\boldsymbol{v}(t) = 0$ in (44) and use the Lyapunov function candidate as given in (51). $V(\boldsymbol{x})$ is positive definite. If we assume perfect collocation between the sensor and actuator pairs, that is $C = B^TP$, the time derivative of $V(\boldsymbol{x})$ along the closed-loop system trajectory becomes

$$\begin{aligned}\dot{V}(\boldsymbol{x}) &= -\boldsymbol{y}_u^TG_p\boldsymbol{y}_u - \tfrac{1}{2}\boldsymbol{x}^TQ\boldsymbol{x} \\ &= -\boldsymbol{x}^T(C^TG_pC + \tfrac{1}{2}Q)\boldsymbol{x}, \end{aligned} \quad (66)$$

where the $n \times n$ diagonal positive semidefinite matrix Q is given in (53). It can be demonstrated by inspection that

$$C^TG_pC + \tfrac{1}{2}Q \geq 0, \quad (67)$$

since the first term in (67) is in quadratic form for diagonal $G_p > 0$ and hence positive semidefinite. The time derivative of $V(\boldsymbol{x})$ is negative semidefinite. Using the invariant set theorem (Vidyasagar, 1993) the equilibrium point of the closed-loop system is asymptotically stable and the result follows. □

L_2^m and L_∞^m stability of the closed-loop system using collocated sensor and actuator pairs is maintained regardless of the number of modes, and regardless of the inaccuracy in the knowledge of the parameters. Thus, the spillover

problem is eliminated and the parameters do not have to be known in advance for stability to be obtained. Notice that there are no restrictions on the location of the collocated sensor and actuator pairs with respect to stability. However, for optimizing the performance the longitudinal location of the sensor actuator pairs is crucial, as seen in equation (27). Robustness with respect to unmodelled dynamics and sector nonlinearities in the actuators are shown in Sørensen (1993). It is further shown by Sørensen (1993) that some imprecision in the collocated sensor and actuator pairs can be accepted without violating the stability properties of the closed-loop system.

4. SIMULATION AND FULL-SCALE RESULTS

In this section numerical simulations and results from full-scale trials with a 35 m SES advancing at high speed in head sea waves are presented. The effect of collocation and noncollocation of the sensor and actuator pairs for the 35 m SES is investigated. The SES is equipped with one single fan and louver system. Main dimensions and data of the SES craft are given in Appendix A. The number of acoustic modes considered in the simulation model is four, i.e. $k = 4$.

4.1. *Numerical simulations*

Figure 5 shows the Bode plot of $H_p(i\omega_e)$ between the pressure sensor $y_u(s)$ and the louver $u(s)$ when the pressure sensor and actuator pair is fully collocated. The sensor and louver are located at the fore end of the air cushion. When the frequency of encounter goes to zero, the dynamic pressure tends to a static value proportional to K_1/K_2. This indicates that the equilibrium pressure p_o will decrease when the equilibrium leakage area increases, and vice versa. Around 0.2 Hz the response is close to zero. This is related to the structural mass forces acting on the SES and the hydrodynamic forces acting on the side-hulls. The high value around 2 Hz is due to the resonance of the dynamic uniform pressure. The high values around 6, 12, 18 and 24 Hz are related to the four acoustic resonance modes. From the phase plot we observe that the phase varies between 90° to −90° in the whole frequency range. This is to be expected when using collocated sensor and actuator pairs.

Figure 6 shows the Bode plots of $H_p(i\omega_e)$ when the pressure sensor is located at the fore end of the air cushion while the louver is located at the aft end of the air cushion. From the phase plot we observe that the sensed pressure signal at the fore end is 180° out of phase compared to the pressure signal at the aft end where the louver is located. This is to be expected with noncollocated sensor and louver pairs. Noncollocated sensor and actuator pairs introduce negative phase and may lead to instability.

4.2. *Full-scale results*

The prototype ride control system used in the full-scale experiments was based on the passive controller as presented in Section 3. The control

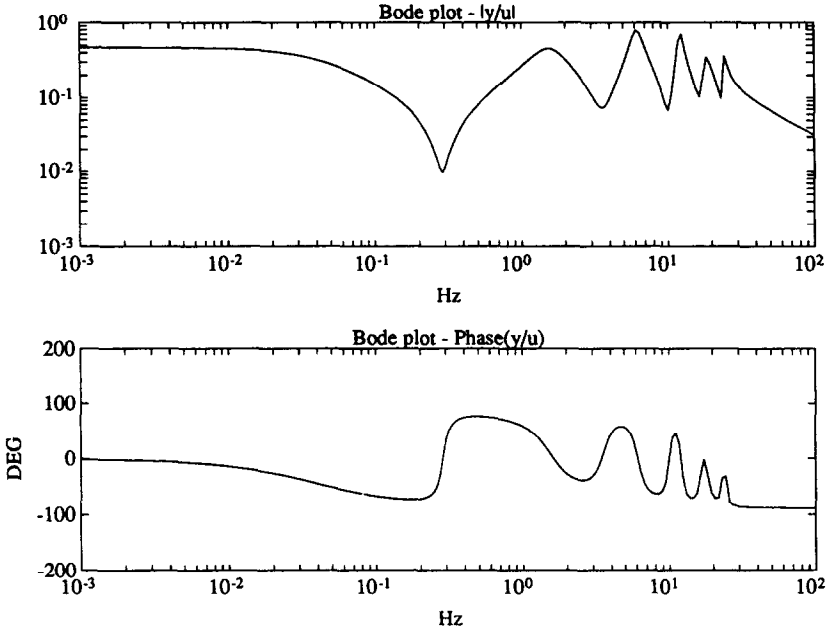

Fig. 5. Collocated sensor and actuator pair; numerically calculated Bode plot of $H_p(i\omega_e)$; $x_L = x_s = 12$ m, $x_F = 6$ m, $U = 50$ knots, $p_o = 500$ mm Wc.

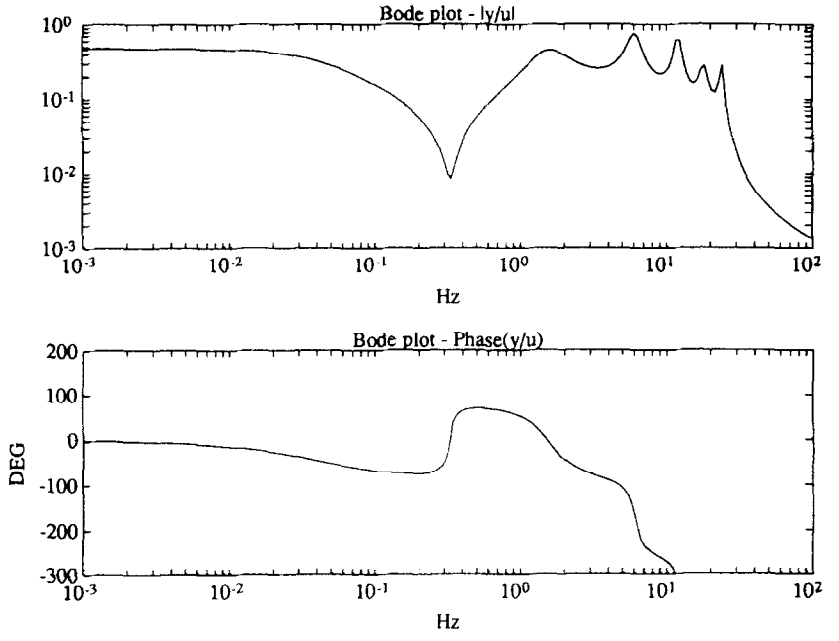

Fig. 6. Noncollocated sensor and actuator pair; numerically calculated Bode plot of $H_p(i\omega_e)$; $x_s = 12$ m, $x_L = -12$ m, $x_F = 6$ m, $U = 50$ knots, $p_0 = 500$ mm Wc.

algorithms in the ride control system were partly implemented on a personal computer (PC). Analog hardware devices were also used. An outer feedback loop was implemented on the PC, while a faster inner feedback loop around the electrohydraulic louver system was implemented by means of analog hardware devices. The louver system consisted of two vent valves located side by side at the same longitudinal position $x_L = 8$ m. The two vent valves were operated in parallel in the outer feedback loop. Two pressure sensors located at $x_{s1} = 10$ m and $x_{s2} = -10$ m were used to measure the excess pressure variations in the air cushion. One accelerometer located about 5 m aft of the centre of gravity was used to measure the vertical accelerations. The inner analog controller loop around the louver system provided the necessary opening and closing actions of the vent valves. The experimental arrangement is illustrated in Fig. 7. The full-scale measurements were carried out in sea states with significant wave heights estimated to vary between 0.3 and 0.6 m. The power spectra of the vertical accelerations with and without the ride control system are presented.

Figure 8 shows the full-scale power spectra of the vertical accelerations about 5 m aft of the centre of gravity with and without the ride control system activated. With the ride control system turned off, we observed significant response around 2, 5 and 8 Hz. The response around 2 Hz is related to the resonance of the dynamic uniform pressure, while the response around 5 and 8 Hz is related to the first odd and even resonance modes. When activating the ride control system the response around 5 Hz was significantly amplified, while the response around 2 Hz was only slightly reduced. In this case the pressure signal at $x_{s2} = -10$ m was used in the feedback loop. Hence, the actuator and sensor pair was completely noncollocated since the louver was located at $x_L = 8$ m. This means that for the first odd mode, the noncollocation resulted in positive feedback for this particular mode because the pressure at the sensor location was 180° out of phase compared to the pressure at the actuator location in the frequency range

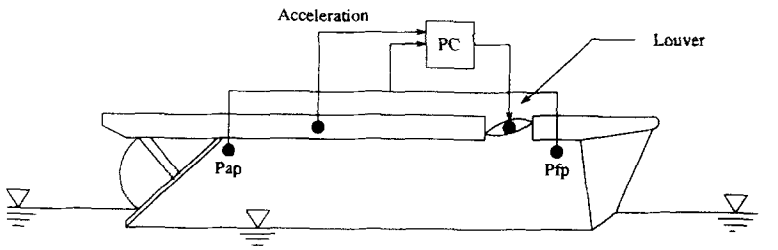

Fig. 7. Experimental arrangement.

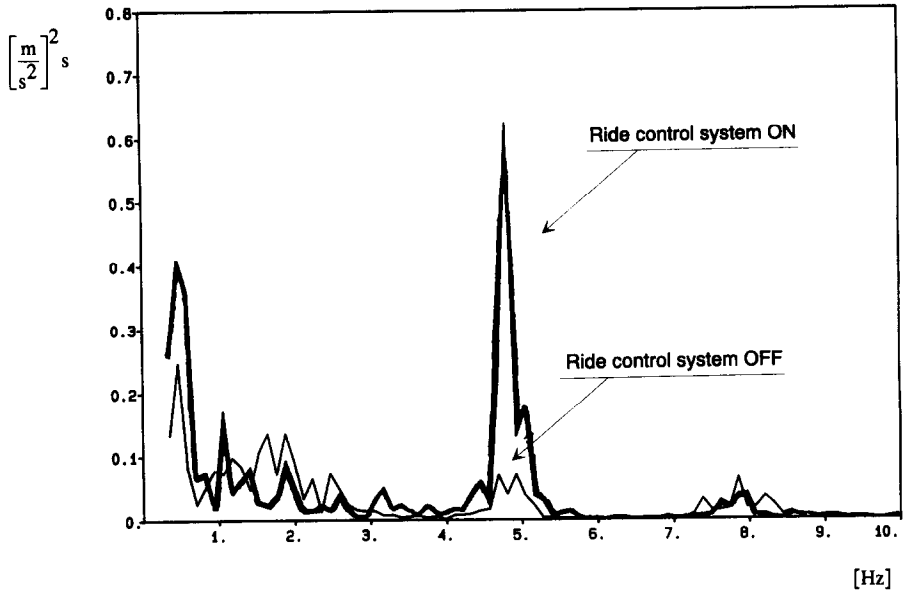

Fig. 8. Noncollocated sensor and actuator pair; full-scale power spectra of the vertical accelerations at $x = -5$ m of a 35 m SES with the ride control system on and off; $p_o = 450$ mm Wc.

dominated by the first odd acoustic resonance mode. The response around 8 Hz was more or less unchanged. Both time series were recorded when the craft was advancing with the speed $U = 45$ knots in head sea waves with significant wave height estimated to be $H_s = 0.3$ m.

Figure 9 shows the full-scale power spectra of the excess pressure variations at $x_{s1} = 10$ m in the air cushion with and without the ride control system activated. The time series were recorded during the same run as above. The pressure signal at $x_{s2} = -10$ m was used in the feedback loop. Hence, the louvers and sensors were completely noncollocated. With the ride control system turned off, we observed a response around 2 and 5 Hz. Activating the ride control system, the response around 5 Hz was significantly amplified. At the resonance of the dynamic pressure around 2 Hz the response level was reduced by the ride control system.

Figure 10 shows the full-scale power spectra of the vertical accelerations about 5 m aft of the centre of gravity with and without the ride control system activated. In this case the pressure signal at $x_{s1} = 10$ m was used in the feedback loop. Hence, the louvers and sensors were 'almost' collocated since the louvers were located at $x_L = 8$ m. With the ride control system

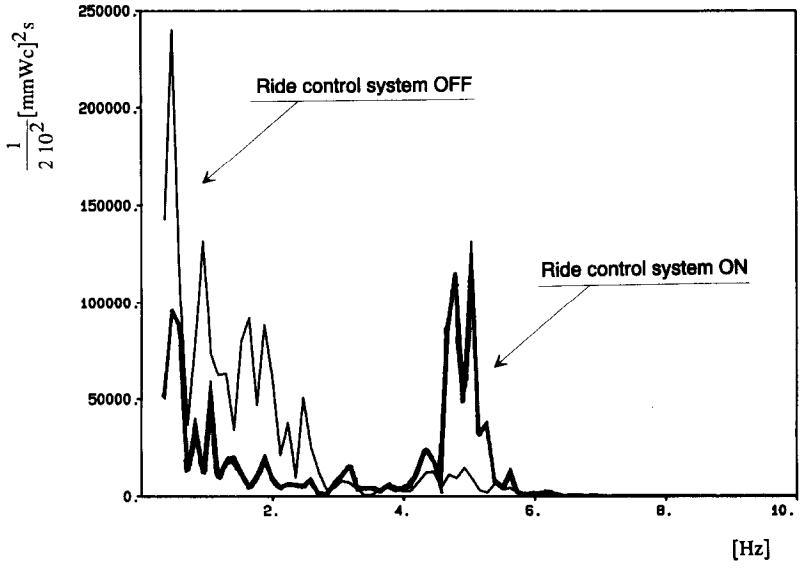

Fig. 9. Noncollocated sensor and actuator pair; full-scale power spectra of the excess pressure at $x = 10$ m of a 35 mm SES with ride control system on and off; $p_o = 450$ mm Wc.

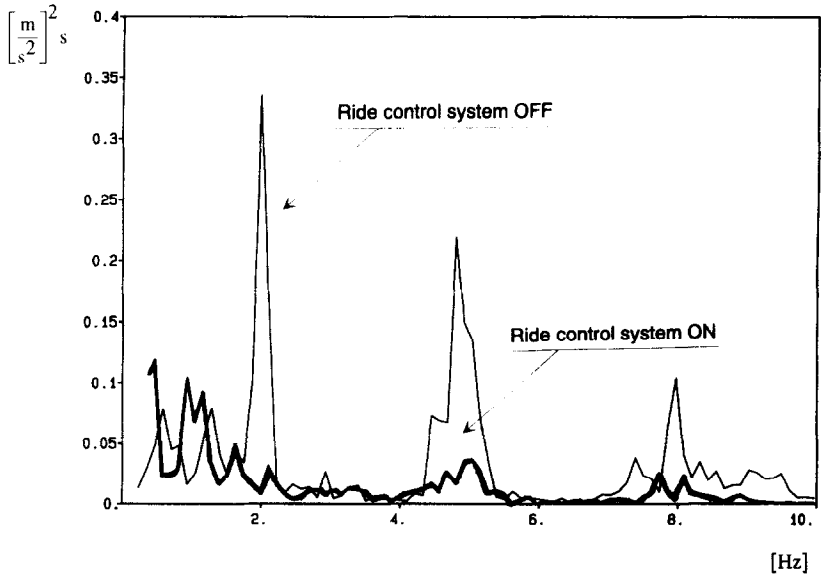

Fig. 10. Collocated sensor and actuator pair; full-scale power spectra of the vertical accelerations at $x = -5$ m SES with ride control system on and off; $p_o = 430$ mmWc.

turned off, we observed responses around 2, 5 and 8 Hz. Activating the ride control system, the response around all three resonance frequencies was significantly reduced. These time series were recorded when the craft was advancing with the speed $U = 44$ knots in head sea waves with significant wave height estimated to be $H_s = 0.6$ m.

Figure 11 shows the full-scale power spectra of the excess pressure variations at $x_{s1} = 10$ m in the air cushion with and without the ride control system activated. The time series were recorded during the same run as in Fig. 10. The pressure signal at $x_{s1} = 10$ m was used in the feedback loop. Hence, the louvers and sensors were 'almost' collocated. With the ride control system turned off, we observed response around 2 and 5 Hz at the fore end of the air cushion. Activating the ride control system, the response around all three resonance frequencies was significantly reduced.

5. CONCLUSIONS

The pressure variations in the pressurized air cushion of a SES have two fundamental characteristics; a dynamic uniform and a spatially varying pressure term. It has been demonstrated

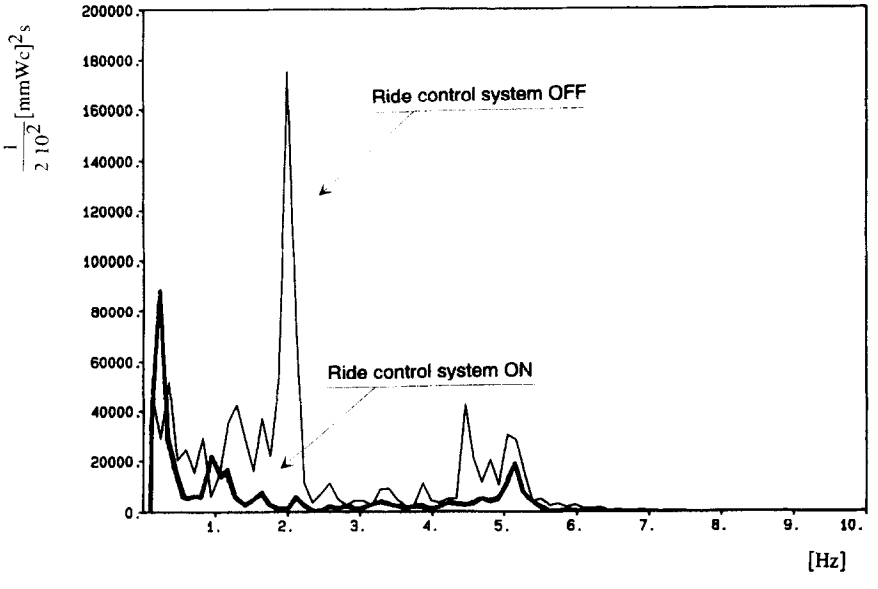

Fig. 11. Collocated sensor and actuator pair; full-scale power spectra of the excess pressure at $x = 10$ m of a 35 mm SES with ride control system on and off; $p_o = 430$ mm Wc.

that the resonances of the dynamic uniform pressure and the spatially varying pressure cause excessive vertical accelerations when the craft is advancing in sea states which contain energy in the frequency domains corresponding to the resonance frequencies. In order to achieve high human comfort and crew workability, it is necessary to reduce these accelerations using a ride control system. A distributed ride control system has been developed based on the theory of passive systems, and a proportional pressure feedback controller has been proposed. Full-scale experiments of a prototype ride control system showed significant improvement in ride quality when using a ride control system which provided dissipation of energy around the resonance frequencies. The full-scale experiments also showed the importance of using collocated sensor and actuator pairs in the acoustic dominated frequency range. Spillover effects such as unwanted excitation of residual modes were avoided, regardless of the number of modes considered and the parameter values, through the use of collocated sensor and actuator pairs.

Acknowledgements—This work has been sponsored by the Ulstein group and the Royal Norwegian Council for Scientific and Industrial Research (NTNF). The authors are grateful to Dr Ole J. Sørdalen, Dr Sverre Steen, Dr Thor I. Fossen and Dr Odd M. Faltinsen at the Norwegian Institute of Technology for valuable discussions.

REFERENCES

Balas, M. (1978). Feedback control of flexible systems. *IEEE Trans. Autom. Contr.*, **AC-23,** 673–679.

Desoer, C. A. and M. Vidyasagar (1975). *Feedback Systems: Input-Output Properties.* Academic Press, New York.

Faltinsen, O. M. (1990). *Sea Loads on Ships and Offshore Structures.* Cambridge University Press, Cambridge.

Faltinsen, O. M. and R. Zhao (1991a). Numerical predictions of ship motions at high forward speed. *Phil. Trans. R. Soc.* Series A, pp. 241–252.

Faltinsen, O. M. and R. Zhao (1991b). Flow predictions around high-speed ships in waves. *Mathematical Approaches in Hydrodynamics,* SIAM.

Faltinsen, O. M., J. B. Helmers, K. J. Minsaas and R. Zhao (1991). Speed Loss and Operability of Catamarans and SES in a Seaway. In *Proc. First International Conference on Fast Sea Transportation—FAST'91,* Trondheim, Norway.

Faltinsen, O. M., J. Hoff, J. Kvålsvold and R. Zhao (1992). Global loads on high-speed catamarans. *PRADS'92,* Newcastle, U.K.

Gelb, A. and W. E. Vander Velde (1968). *Multiple-Input Describing Functions and Nonlinear System Design.* McGraw-Hill, New York.

Gevarter, W. B. (1970). Basic relations for control of flexible vehicles. *AIAA J.,* **8,** pp. 666–672.

Haddad, W. M., D. S. Bernstein and W. Wang (1993). Dissipative H^2/H^∞ controller synthesis. In *Proc. Am. Contr. Conf.,* San Francisco, CA.

Joshi, S. M. (1989). *Control of Large Flexible Space Structures.* Springer, Berlin.

Joshi, S. M. and P. G. Maghami (1990). Dissipative compensators for flexible spacecraft control. In *Proc. Am. Contr. Conf.,* San Diego, CA.

Joshi, S. M., P. G. Maghami and A. G. Kelkar (1991). Dynamic dissipative compensator design for large space structures. *AIAA Guidance, Navigation, Contr. Conf.,* New Orleans, LA.

Kaplan, P. and S. Davis (1974). A simplified representation of the vertical plane dynamics of SES craft. *AIAA Paper No.* 74–314, AIAA/SNAME *Adv. Marine Vehicles Conf.,* San Diego, California.

Kaplan, P. and S. Davis (1978). System analysis techniques for designing ride control system for SES craft in waves. *5th Ship Contr. Syst. Symp.,* Annapolis, MD.

Kaplan, P., J. Bentson and S. Davis (1981). Dynamics and hydrodynamics of surface effect ships. *Trans. SNAME,* **89,** pp. 211–247.

Keener, J. P. (1988). *Principles of Applied Mathematics.* Addison-Wesley, Redwood City, CA.

Lozano-Leal, R. and S. M. Joshi (1988). On the design of dissipative LQG-type controllers. In *Proc. 27th IEEE Conf. Decision Contr.,* TX.

Nestegård, A. (1990). Motions of surface effect ships. A. S. Veritas Research Report No.: 90–2011.

Salvesen, N., E. O. Tuck and O. M. Faltinsen (1970). Ship motions and sea loads. *Trans. SNAME,* **78,** 345–356.

Sørensen, A. J., S. Steen and O. M. Faltinsen (1993). Cobblestone effect on SES. *High Performance Marine Vehicle Conf.*—HPMV'92, ASNE, Washington D.C.

Sørensen, A. J., S Steen and O. M. Faltinsen (1993). SES dynamics in the vertical plane. *J. Ship Techn. Res.,* **40,** pp. 71–94.

Sørensen, A. J. (1993). Modelling and Control of SES Dynamics in the Vertical Plane. Dr. Ing. Thesis, Department of Engineering Cybernetics, the Norwegien Institute of Technology.

Vidyasagar, M. (1993). *Nonlinear System Analysis,* 2nd Edn Prentice Hall, Englewood Cliffs, NJ.

APPENDIX A

SES main dimensions
Length overall: 35 m
Equilibrium fan flow rate: 150 m^3/s
Linear fan slope: $-140\ m^2/s$
Cushion length: 28 m
Nom. cushion pressure: 500 mm Wc
Cushion beam: 8 m
Cushion height: 2 m
Weight: 150 ton
Speed: 50 knots

APPENDIX B

Boundary conditions

We can set up the following boundary conditions on the surfaces enclosing the cushion air volume.

1. On the rigid part of the wetdeck ($z = h_o$)

$$\frac{\partial \phi_{sp}(x, z, t)}{\partial z} = \dot{\eta}_3(t) - x\dot{\eta}_5(t). \tag{B.1}$$

2. At the rigid bow and rear seal systems ($x = \pm L/2$)

$$\frac{\partial \phi_{sp}(x, z, t)}{\partial x} = 0. \tag{B.2}$$

3. At the fan outlet ($z = h_o, x = x_{Fi}$)

$$\frac{\partial \phi_{sp}(x, z, t)}{\partial z} = -p_o \sum_{i=1}^{q} \frac{1}{A_{Fi}} \frac{\partial Q}{\partial p}\bigg|_{oi} \left(\sum_{j=1}^{\infty} \dot{p}_j(t) r_j(x_{Fi}) + \mu_u(t) \right), \tag{B.3}$$

where A_{Fi} is the outlet area of fan i.

4. At the controlled leakage area ($z = h_o, x = x_{Li}$)

$$\frac{\partial \phi_{sp}(x, z, t)}{\partial z} = c_n \sqrt{\frac{2\rho_o}{\rho_a}} \sum_{i=1}^{r} \left(\tfrac{1}{2} \sum_{j=1}^{\infty} \dot{p}_j(t) r_j(x_{Li}) + \tfrac{1}{2}\mu_u(t) - \frac{\Delta A_i^{RCS}(x_{si}, t)}{A_{oi}^{RCS}} \right). \tag{B.4}$$

5. At the bow leakage area ($z = 0, x = x_{FP} = L/2$)
Assuming no motion induced leakage, we have

$$\frac{\partial \phi_{sp}(x, z, t)}{\partial z} = -\frac{c_n}{2} \sqrt{\frac{2p_o}{\rho_a}} \left(\sum_{i=1}^{\infty} \dot{p}_j(t) r_j(x_{FP}) + \mu_u(t) \right). \tag{B.5}$$

6. At the stern leakage area ($z = 0, x = x_{AP} = -L/2$)
Assuming no motion induced leakage, we have

$$\frac{\partial \phi_{sp}(x, z, t)}{\partial z} = -\frac{c_n}{2} \sqrt{\frac{2p_o}{\rho_a}} \left(\sum_{j=1}^{\infty} \dot{p}_j(t) r_j(x_{AP}) + \mu_u(t) \right). \tag{B.6}$$

7. At the mean free surface ($z = 0$)

$$\frac{\partial \phi_{sp}(x, z, t)}{\partial z} = \omega_e \zeta_a \cos(kx + \omega_e t). \tag{B.7}$$

APPENDIX C

Symbolic model matrices
The $n \times n$ system is given by

$$A = \begin{bmatrix} A1_{5\times5} & 0_{5\times k} & A2_{5\times k} \\ 0_{k\times5} & 0_{k\times k} & I_{k\times k} \\ A3_{k\times5} & A4_{k\times k} & A5_{k\times k} \end{bmatrix}, \tag{C.1}$$

where $0_{5\times k}$, $0_{k\times5}$ and $0_{k\times k}$ are the $5\times k$, $k\times5$ and $k\times k$ zero matrices, respectively. $I_{k\times k}$ is the $k\times k$ identity matrix. $A1_{5\times5}$ is defined as

$$A1_{5\times5} = \begin{bmatrix} 0 & 0 & 1 & 0 & 0 \\ 0 & 0 & 0 & 1 & 0 \\ -\dfrac{C_{33}}{m + A_{33}} & 0 & -\dfrac{B_{33}}{m + A_{33}} & 0 & \dfrac{A_c p_o}{m + A_{33}} \\ 0 & -\dfrac{C_{55}}{I_{55} + A_{55}} & 0 & -\dfrac{B_{55}}{I_{55} + A_{55}} & 0 \\ 0 & 0 & -\dfrac{\rho_{co} A_c}{K_1} & 0 & -\dfrac{K_3}{K_1} \end{bmatrix}. \tag{C.2}$$

$A2_{5\times k}$ is defined as

$$A2_{5\times k} = \begin{bmatrix} 0 & 0 & 0 & 0 & 0 & \cdots & 0 \\ 0 & 0 & 0 & 0 & 0 & \cdots & 0 \\ 0 & 0 & 0 & 0 & 0 & \cdots & 0 \\ d_1 & 0 & d_3 & 0 & d_5 & \cdots & 0 \\ 0 & 0 & 0 & 0 & 0 & \cdots & 0 \end{bmatrix}, \tag{C.3}$$

where

$$d_j = \frac{2p_o b}{I_{55} + A_{55}} \left(\frac{L}{j\pi} \right)^2. \tag{C.4}$$

$A3_{k\times5}$ is defined as

$$A3_{k\times5} = \begin{bmatrix} 0 & 0 & 0 & g_1 & 0 \\ 0 & 0 & 0 & 0 & 0 \\ 0 & 0 & 0 & g_3 & 0 \\ \vdots & \vdots & \vdots & \vdots & \vdots \\ 0 & 0 & 0 & 0 & 0 \end{bmatrix}, \tag{C.5}$$

where

$$g_j = -\frac{4\rho_{co} L c^2}{p_o h_o (j\pi)^2}. \tag{C.6}$$

$A4_{k\times k}$ and $A5_{k\times k}$ are defined as

$$A4_{k\times k} = \text{diag}\,[-\omega_j^2], \tag{C.7}$$

$$A5_{k\times k} = \text{diag}\,[-2\xi_j\omega_j]. \tag{C.8}$$

The $n \times (3+k)$ disturbances matrix is defined as

$$E = \begin{bmatrix} 0 & 0 & 0 & 0 & 0 & \cdots & 0 \\ 0 & 0 & 0 & 0 & 0 & \cdots & 0 \\ \dfrac{1}{m+A_{33}} & 0 & 0 & 0 & 0 & \cdots & 0 \\ 0 & \dfrac{1}{I_{55}+A_{55}} & 0 & 0 & 0 & \cdots & 0 \\ 0 & 0 & \dfrac{\rho_{co}}{K_1} & 0 & 0 & \cdots & 0 \\ & & 0_{k\times(3+k)} & & & & \\ & 0_{k\times 3} & & & \rho_{co}I_{k\times k} & & \end{bmatrix}. \tag{C.9}$$

The $n \times r$ control input matrix is given by

$$B = \begin{bmatrix} 0 & 0 & \cdots & 0 \\ 0 & 0 & \cdots & 0 \\ 0 & 0 & \cdots & 0 \\ 0 & 0 & \cdots & 0 \\ \dfrac{K_2}{K_1} & \dfrac{K_2}{K_1} & \cdots & \dfrac{K_2}{K_1} \\ & 0_{k\times r} & & \\ c_1\cos\dfrac{\pi}{L}\left(x_{L1}+\dfrac{L}{2}\right) & c_1\cos\dfrac{\pi}{L}\left(x_{L2}+\dfrac{L}{2}\right) & \cdots & c_1\cos\dfrac{\pi}{L}\left(x_{Lr}+\dfrac{L}{2}\right) \\ c_1\cos\dfrac{2\pi}{L}\left(x_{L1}+\dfrac{L}{2}\right) & c_1\cos\dfrac{2\pi}{L}\left(x_{L2}+\dfrac{L}{2}\right) & \cdots & c_1\cos\dfrac{2\pi}{L}\left(x_{Lr}+\dfrac{L}{2}\right) \\ \vdots & & & \\ c_1\cos\dfrac{k\pi}{L}\left(x_{L1}+\dfrac{L}{2}\right) & c_1\cos\dfrac{k\pi}{L}\left(x_{L2}+\dfrac{L}{2}\right) & \cdots & c_1\cos\dfrac{k\pi}{L}\left(x_{Lr}+\dfrac{L}{2}\right) \end{bmatrix}. \tag{C.10}$$

The $m \times n$ measurement matrix is given by

$$C^{\mathrm{T}} = \begin{bmatrix} 0 & 0 & \cdots & 0 \\ 0 & 0 & \cdots & 0 \\ 0 & 0 & \cdots & 0 \\ 0 & 0 & \cdots & 0 \\ 1 & 1 & \cdots & 1 \\ & 0_{k\times m} & & \\ \cos\dfrac{\pi}{L}\left(x_{s1}+\dfrac{L}{2}\right) & \cos\dfrac{\pi}{L}\left(x_{s2}+\dfrac{L}{2}\right) & \cdots & \cos\dfrac{\pi}{L}\left(x_{sm}+\dfrac{L}{2}\right) \\ \cos\dfrac{2\pi}{L}\left(x_{s1}+\dfrac{L}{2}\right) & \cos\dfrac{2\pi}{L}\left(x_{s2}+\dfrac{L}{2}\right) & \cdots & \cos\dfrac{2\pi}{L}\left(x_{sm}+\dfrac{L}{2}\right) \\ \vdots & & & \\ \cos\dfrac{k\pi}{L}\left(x_{s1}+\dfrac{L}{2}\right) & \cos\dfrac{k\pi}{L}\left(x_{s2}+\dfrac{L}{2}\right) & \cdots & \cos\dfrac{k\pi}{L}\left(x_{sm}+\dfrac{L}{2}\right) \end{bmatrix}, \tag{C.11}$$

where

$$c_1 = \frac{2K_2c^2}{p_oV_{co}}. \tag{C.12}$$